NEAR-FIELD MEASUREMENT AND MODELING RESULTS FOR A FLIGHT-TYPE ARCJET: NH MOLECULE

Mark W. Crofton and Teresa A. Moore
Technology Operations, The Aerospace Corporation
M5/754, P.O. Box 92957, Los Angeles, California, 90009, U.S.A.

Iain D. Boyd
Department of Aerospace Engineering, University of Michigan
Ann Arbor, Michigan, 48109-2140, U.S.A.

Ideo Masuda
DRTS Project Team, National Space Development Agency of Japan
2-1-1 Sengen, Tsukuba, Ibaraki, 305-8505, Japan

Yoshifumi Gotoh
Space Systems Department, Mitsubishi Electric Corporation
325, Kamimachiya Kamakura, Kanagawa 247, Japan

Abstract

Density, velocity, and temperature data were obtained in the near-field plume of an MR-509A arcjet thruster, using the NH molecule as a probe. The arcjet, a 1.8 kW model manufactured by PRIMEX Aerospace, will operate on the DRTS spacecraft being developed by Mitsubishi Electric Corporation. The arcjet was run on an N_2/H_2 gas mix simulating hydrazine decomposition products. Plume measurements were made spanning the region from nozzle exit plane to the free molecular flow regime.

The NH measurements utilized a resonant laser-induced fluorescence transition originating from the ground electronic state. Although a similar laser-induced fluorescence study had been performed on an ammonia arcjet, this was the first on a flight-type device. The rotational temperature of NH was obtained in v=0,1 of the electronic ground state, and vibrational population in v=1,2. Temperature variation along the thrust axis was minor, and rotational and vibrational temperatures were similar. Lineshapes as well as radial and axial profiles of the peak line intensity were obtained. Maximum signal was obtained on-axis 1.4 cm downstream from the exit plane. Axial velocity components were determined at various plume locations. Direct Simulation Monte Carlo (DSMC) predictions have been generated for comparison with much of the experimental data and to provide additional flowfield information. Good agreement was achieved in most cases.

Nomenclature

a	Gaussian normalization parameter
b	Gaussian linewidth parameter
B_{12}	Einstein coefficient for absorption, 1→2
c	speed of light
e	elementary charge
Erot	rotational energy of the originating state
f	oscillator strength
g(ν)	Gaussian lineshape function
$\hbar$	Planck's constant divided by 2π
I_ν	intensity of photon flux at frequency ν
I	intensity of photon flux
k_ν	absorption coefficient at frequency ν
K	proportionality constant
L	absorption pathlength
m	electron mass
M	species molar mass
N_i	density of species i
N_l	population density of lower level
r	radial coordinate
T	temperature, K
z	axial coordinate
Δt_L	duration of laser pulse
$\Delta\nu_D$	Doppler Full-Width-Half-Maximum (FWHM)
ν	frequency
ν_0	center frequency
ρ	radiation density
σ	absorption cross section
ω	angular frequency

Subscripts

D	Doppler
l	laser
S	Stark effect
P	Power broadening
SAT	saturation
SA	self-absorption

Introduction

MR-509A/B hydrazine arcjet thrusters[1] will provide north-south stationkeeping for the Data Relay Test Satellites (DRTS) being developed for on-orbit operation commencing in 2001 and 2002. MELCO is the prime contractor to NASDA for DRTS. Despite the successful operation of PRIMEX Aerospace Corporation (PAC) arcjets on several U.S. satellites,[2] little quantitative information has been available concerning many of the thruster impacts on satellites of arbitrary configuration. To rectify this situation for the DRTS case, MELCO contracted with The Aerospace

Copyright © 1999 by the Japan Society for Aeronautical and Space Sciences. All rights reserved.

Corporation to perform experimental measurements coupled with theoretical analyses. This resulted in the first laser-induced fluorescence and mass spectrometric studies for a flight-type arcjet thruster. A portion of the Aerospace experimental work concerned with the measurement of near-field parameters is described in this report.

Limited time was available for data gathering on the MR509A. This curtailed the data set that could otherwise have been obtained.

Experimental Setup

Test Facility and Arcjet Operation

All experimental testing was performed at The Aerospace Corporation's Mechanics and Materials Technology Center. The test chamber is 5.5 m in length and 2.4 m in diameter. Two custom 1.2 m CVI reentrant cryopumps which hang inside the chamber, suspended from flanges, were inactive during arcjet operation (the chamber has since been upgraded in its size and pumping speed). Test chamber vacuum was maintained by 16 VHS-400 diffusion pumps. During thruster operation at the nominal flow rate of 46.4 mg/s, test chamber background pressure was maintained below 1×10^{-3} Torr.

The thruster was mounted on a computer-controlled four-axis positioning system. The thruster axis could rotate in a horizontal plane more than 20 deg off the test chamber axis on one side and up to 10 deg on the other. This degree of freedom was not necessary during the LIF measurements; the arcjet nozzle was aligned with the long axis of the test chamber and remained there. The vertical position of the arcjet was similarly fixed for the duration of the measurements. Two-axis positioning was performed in the axial and radial directions to explore the spatial dependence of near-field parameters.

Electrical power of 1.8 kW was supplied at 80 VDC to the power conditioning unit provided by PAC. Power was similarly supplied at 28 VDC to operate the protection and control electronics which had also been provided by PAC. These were not the flight-model units. The flight-model power processing unit for DRTS requires an input voltage of 33-51.5 VDC.[1]

A computer-controlled data acquisition and control system was supplied by Aerospace and set up to satisfy PAC specifications regarding arcjet operating limits. Arcjet operating voltage, current, inlet pressure, and flow rates were monitored at all times, and an automatic shutdown would have occurred had any process limit been exceeded during normal operations. Typical recorded parameters at the 46.4 mg/s nominal operating point at which all H and NH data were obtained are listed in Table 1. In practice, voltage and current levels varied somewhat but the power conditioner kept arcjet input power constant at 1.66 kW.

Table 1. Typical operating parameters during LIF measurements of H and NH in the MR-509 plume.

Flow rate	Background Press.	Arc Voltage	Arc Current	Input Power	Thrust[a]	I_{sp}[a]
46.4 mg/s	0.8 mTorr	109.7 V	15.1 A	1.66 kW	235 mN	517 s

[a]Estimated from flight qualification data of Ref. 3, with 2% reduction for use of simulated N_2H_4 (2:1 mix of H_2,N_2)

Laser-Induced Fluorescence

Laser-Induced Fluorescence (LIF) is the preferred means of obtaining the near-field parameters discussed in this report. LIF offers high spatial resolution together with high sensitivity and results which are acceptable from a quantitative standpoint. Sub-millimeter spatial resolution is a requirement in the near-field, since the arcjet nozzle width at the exit plane is on the order of a centimeter. Sensitivity is a factor at the existing species densities, which range from 10^{12}-10^{16} cm^{-3} in the probed region.

For the NH data set, a one-photon absorption process was employed. In the limit of low laser power, the one-photon LIF signal intensity of a two level system can be expressed as[4]

$$I = KN_l B_{12} \rho \Delta t_L \qquad (1)$$

The constant K accounts for the details of the detection system and averaging of the laser field vector projection onto the transition dipole vector.

By determining relative quantum state populations, rotational and vibrational temperatures can be found. The relative populations of lower levels j and k may be found by using Equ. (1) to form the ratio

$$\frac{n_j}{n_k} = \frac{[B_{12}\rho]_k I_j}{[B_{12}\rho]_j I_k} \qquad (2)$$

where any variation of detector response with frequency has been neglected. This equation is again valid in the limit of low laser power, but it holds for all cases where the laser power is the same for transitions from j and k, and the B coefficients for j and k are identical. Since the population is proportional to $(2J+1)e^{-E_{rot}/kT}$, the rotational temperature of the lower state can, in favorable cases, be determined from the relation

$$\ln\left(\frac{I}{2J+1}\right) \cong \ln C - \frac{E_{rot}}{kT} \; . \qquad (3)$$

In the more general case for which laser pulse intensity is kept constant but the B coefficients vary over the series and the transitions are not fully saturated, 2J+1 in Equ. (3) must be replaced by an expression depending on S_J, the line strength factor. Measurements of relative transition intensity for determination of rotational and vibrational temperature were made at pulse energy levels approaching the saturation limit (right side of Fig. 1), and temperatures were obtained without the use of line strength factors.

Because of the large transition moment of the A $^3\Pi$ - X $^3\Sigma^-$ transition (f=0.0075),[5] the < 10 ns duration of the laser pulse and the requirement of sub-mm spatial resolution, it was difficult to eliminate all saturation effects. A measurement of LIF signal intensity from NH over a range of laser pulse energies produced the curve given in Fig. 1. In all cases, pulse energy was determined near the output of the dye laser harmonic doubler. Energy levels at the arcjet itself were approximately 60% of these values. The saturation effect is obvious.

Due to power broadening, the linewidth of NH transitions will be proportional to $(1+I/I_{sat})^{1/2}$.[6] The width of $R_2(7)$ was broadened to 0.4 cm^{-1} at ≈200 μJ pulse energy levels. Pulse energy was ≈ ×50 less for the measurement of peak signal profile on the thrust axis, and composite parallel

and perpendicular lineshapes. Pulse energy was kept constant for the measurements of relative rotational line strength. For the latter data, pulse energy was about 20 μJ. Given the small variation in B coefficients and saturation of the transitions, 2J+1 was used in Equ. (3) for the temperature determinations, rather than S_J.

At low light intensities single photon absorption may be written in differential form as

$$-dI_\nu = \sigma(\nu) I_\nu N_l(x) dx \ , \qquad (4)$$

where *dx* makes an infinetesimal contribution to L.

Quenching of excited states may occur as a result of collisions with partners in other quantum states. This is usually a problem at high gas densities. For the arcjet, the sum of species densities at the nozzle exit plane is about 8×10^{15} cm^{-3}. In LIF measurements, if the upper state lifetime is much shorter than the interval between quenching collisions, quenching effects can be neglected. The NH molecule has a lifetime in the A $^3\Pi$ excited state of about 400 ns.[7,8] During an interval of 400 ns, NH molecules moving along the plume axis at 7 km/s travel 2.8 mm. The laser beam was positioned to traverse the plume a short distance (about 1 mm) upstream from the center of the detection zone, in order to reduce the detected laser scatter. With an effective length of the detection zone for NH fluorescence of about 2 mm, NH fluorescence would be largely detected between 100 and 350 ns after initial excitation. This interval was reduced by the boxcar gate, set to span 100-280 ns after the laser pulse. The interval between quenching collisions of an NH molecule with the background gas near the nozzle exit plane is on the order of 1 μs, so that quenching can have some influence on the observed fluorescence. Substantial quenching effects are to be expected inside the nozzle.

The LIF experimental setup assumed several different configurations, depending on the measurement of interest. A YAG-pumped dye laser operating at 40 Hz repetition rate generated ≥ 1 mJ per 6 ns pulse in the region 660-680 nm region, using a DCM/LD700 dye mixture. The dye laser output was doubled in a KDP crystal, which was tuned via a tracking circuit to maintain maximum output despite temperature drifts and frequency tuning.

After elevation to the appropriate height for entry into the vacuum chamber, the laser beam entered through a window and passed through the arcjet plume perpendicular to the arcjet thrust axis. To obtain an axial velocity measurement, an optic placed below the thruster steered the beam to a second optic sitting downstream and below the thrust axis. The latter optic steered the beam to intersect the plume at an angle of 43 deg with respect to the thrust axis, and in the correct location to be aligned with the fluorescence collection optics.

For NH the laser beam was weakly focused to enhance the spatial resolution. Fluorescence was collected by a 5-cm-diameter MgF_2 lens placed 18 cm away from the arcjet centerline. The slowly converging fluorescence beam was transmitted over a distance of 1.2 m to a reflector which steered it through a LiF window into the external environment. The fluorescence beam then passed through a 10 nm bandpass filter and entered a 0.125 m monochromator. Detection was accomplished by means of a Hamamatsu R955 photomultiplier tube attached at the monochromator exit. A boxcar amplifier was used to integrate the signal. Alignment of the collection optics was accomplished using a HeNe laser propagated back from the monochromator entrance, or scattered light from the probe laser at the location of interest.

Table 2. NH parallel and perpendicular translational temperatures from DSMC and experimental data.

(r,Z) cm	Perpendicular Temp (K) DSMC (N atom)	Parallel Temp (K) DSMC (N atom)	Composite Temp (K) DSMC (N atom)	Composite Temp (K) Experiment (NH)
0,0.18	1700	3620	2730	3060 ± 400
0,1.96	620	2410	1580	2420 ± 400

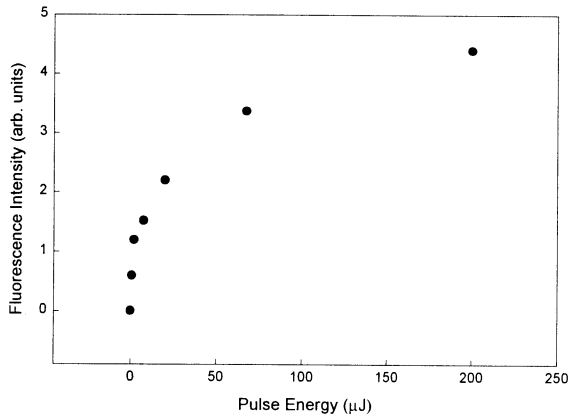

Figure 1. Observed saturation effect of NH $R_2(7)$ v'=0←v"=0, A $^3\Pi \leftarrow$ X $^3\Sigma^-$ transition.

The laser pulse energy generating the fluorescence was recorded together with the fluorescence signal using computerized data acquisition. NH data was usually taken at a constant average energy level, maintained through the use of an attenuator (polarizer-half waveplate combination). NH data were not normalized for power dependence as this was not deemed necessary. Attenuation of the pulse energy was required when measuring radial and axial signal profiles and lineshapes. NH transitions were noticeably broadened at 200 μJ pulse energy. A beamsplitter and neutral density filter combination reduced the pulse energy by a factor of ~30 for lineshapes and axial intensity profiles. Copper sheet was placed over the aluminum thermal shield beneath the arcjet to reduce the level of scattered light. Scattering was a problem for meaurement of the axial intensity profile before installing the copper sheet and attenuating the laser beam.

Lineshapes were obtained by stepping the dye laser frequency, collecting signal for a suitable period, and repeating over the full range of the transition. Fundamental frequencies were obtained in vacuum wavenumbers using a pulsed wavemeter, typically accurate to about 0.01 cm^{-1}. The wavemeter was automatically calibrated at intervals with an internal helium-neon laser, but was subject to minor drifting behavior between calibrations which occasionally

resulted in readout errors of up to 0.03 cm^{-1}. Lineshapes were fitted with a three parameter Gaussian function

$$f = a\exp(-\frac{1}{2}(\frac{\nu-\nu_0}{b})^2) \quad . \tag{5}$$

In many cases the transition center frequency was fixed, but the linewidth parameter and peak height were always variables. These parameters normally showed little dependence on whether the center frequency was fixed. The small residual baseline present in the experimental measurements was subtracted prior to fitting. The linewidth was determined largely by Doppler broadening and laser linewidth. In a few cases power broadening was suspected or known to be large. That data is not included in this report. The Doppler width (FWHM) is determined by the Maxwell-Boltzmann distribution, and is related to temperature by

$$\Delta\nu_D = 2\sqrt{2\ln 2}b_D = 7.162\times10^{-7}\nu_0\sqrt{\frac{T}{M}} \quad , \tag{6}$$

where

$$b_D \cong \sqrt{b^2 - b_L^2 - b_S^2 - b_{SA}^2 - b_P^2} \quad . \tag{7}$$

Since Stark broadening, self-broadening, and power broadening do not give rise to a Gaussian lineshape, Equ. (7) is an approximation only applicable where b_S, b_{SA}, and b_P are effective widths and $b_{SA}^2, b_S^2, b_P^2 << (b_D^2 + b_L^2)$. The translational temperature (Kelvin) may be expressed as

$$T = 1.0811\times10^{13}\frac{M}{\nu_0^2}b_D^2 \quad , \tag{8}$$

where M is the species molar mass in amu and ν_0 is in wavenumbers. The laser linewidth (FWHM) at the fundamental output of the dye laser (565-680 nm) was assumed to be 0.05 cm^{-1} and Gaussian, in approximate agreement with the dye laser specifications and a rough one-time wavemeter analysis. The laser linewidth at the doubled dye laser frequency was assumed to be 0.07 cm^{-1} (0.035 cm^{-1} for plots using the fundamental frequency).

Following the application of self-broadening, quenching, and linewidth corrections, the H atom experimental density profile was in acceptable agreement with the DSMC result.[9] For NH, the difference between the DSMC result and the experimental result is still nearly an order of magnitude after accounting for linewidth and quenching effects.

Quenching of the NH excited state by the background of molecules and atoms in the plume is non-negligible. The rates of quenching by H_2 and N_2 at 1400K have been measured,[10] with the respective rate constants 1.9×10^{-10} cm^3s^{-1} and $< 2 \times 10^{-12}$ cm^3s^{-1}. The quenching rate by H atom is probably $\geq 1.7 \times 10^{-10}$ cm^3s^{-1} at room temperature.[11] Assuming a $T^{1/2}$ dependence for these rate constants at the elevated temperature of the arcjet, quenching by H atom and H_2 occurs at similar rates with the combined rate of 2×10^6 s^{-1}, about equal to the rate of radiative decay. That quenching does occur in the plume was verified by the observed decrease in fluorescence decay time near the exit plane. At the usual boxcar gate setting of 100 ns delay and 180 ns width, the fluorescence decay rate was observed to increase within 3 mm of the exit plane, on-centerline. Because the optical alignment spatially limited the detection of fluorescence, the full fluorescence decay curve could not be observed. It is believed that the effect of quenching on data obtained ≥ 3 mm from the exit plane was small.

Numerical Approach

The flow inside the hydrazine arcjet is characterized by relatively low densities and very high temperatures. The Knudsen number of the nozzle flow (ratio of mean free path to boundary layer scale) varies from about 0.001 at the nozzle throat to about 0.1 at the nozzle exit plane. These values indicate that the flow will be in a state of thermochemical nonequilibrium. At the same time, on the flow axis near to the arc constriction, the ionization level can be as high as 40%.

These conditions place a heavy demand on attempts to perform accurate numerical simulations of the arcjet flow. At Primex, a continuum-based computer code called KARNAC has been developed for computing arcjet flows. The code has performed very well in detail for hydrogen arcjet flows.[12] The accuracy of the code for hydrazine flows is less clear. There are several physical limitations of the KARNAC code. First, all energy modes are assumed to be in equilibrium. This precludes the possibility of freezing of the vibrational and rotational energy modes of the molecular species in the flow (N_2 and H_2). These are known to be loss mechanisms for arcjets. Second, by the time a Knudsen number of 0.1 is reached, the physical basis of the Navier-Stokes equations of fluid mechanics is no longer valid. Finally, because there is no thermal nonequilibrium included, important physical phenomena such as vibration-dissociation coupling are missing.

While we are primarily interested in analysis of the arcjet plume, for the reasons listed above, a more detailed analysis of the nozzle flow is also merited. In the present study, the direct simulation Monte Carlo method (DSMC)[13] is employed to compute both the nozzle and plume flows in a single simulation. The nozzle flow is begun just downstream of the constrictor in a region of the flow that is in the continuum regime. A startline for the DSMC computation is obtained from a solution generated by KARNAC and provided by Primex. The DSMC code includes the following physical phenomena:

(1) multi-species flow (H_2, H, H^+, e^-, N_2, N);

(2) rotational and vibrational relaxation;

(3) dissociation (with vibration coupling), ionization, and recombination reactions;

(4) ohmic heating.

The code is described in detail in Ref. 14 and has been extensively validated against experimental data for hydrogen arcjets.[15]

In terms of boundary conditions, the nozzle wall is treated as being diffuse with full accommodation of all energy modes to a fixed temperature of 1400 K. For the plume expansion, the experimentally determined back-pressure of 0.113 Pa is imposed. The analysis is performed for the nominal operating case of a flow rate of 46.4 mg/s and a power input to the arcjet of 1660 W.

The computation employs a structured grid of 500 by 70 cells. At steady state, a total of about 350,000 particles is employed. The computations provide mean particle quantities such as density, temperature, and velocity. Velocity distribution functions are also computed and this

required the simulations to be performed over an extended period in order to reduce statistical scatter in the distributions collected.

Results and Discussion

NH is a convenient probe species for vibrational, rotational, and translational temperatures in arcjets, as well as velocity and density distributions.[16] In spite of the complete absence of N and NH in the Karnac results, the mass spectrometry data indicates mole fractions in the far-field of 6 and 1.5 %, respectively.[17] NH was not included in the DSMC calculations due to its small abundance relative to N_2 and the planned use of N_2 as a near-field probe. In retrospect it would have been useful for NH to be included in the simulations.

The lineshapes obtained for NH are plotted in Fig. 2, along with their Gaussian fits. In each case, the laser beam intersected the plume centerline at an angle of about 42.8 deg., resulting in a composite of perpendicular and parallel

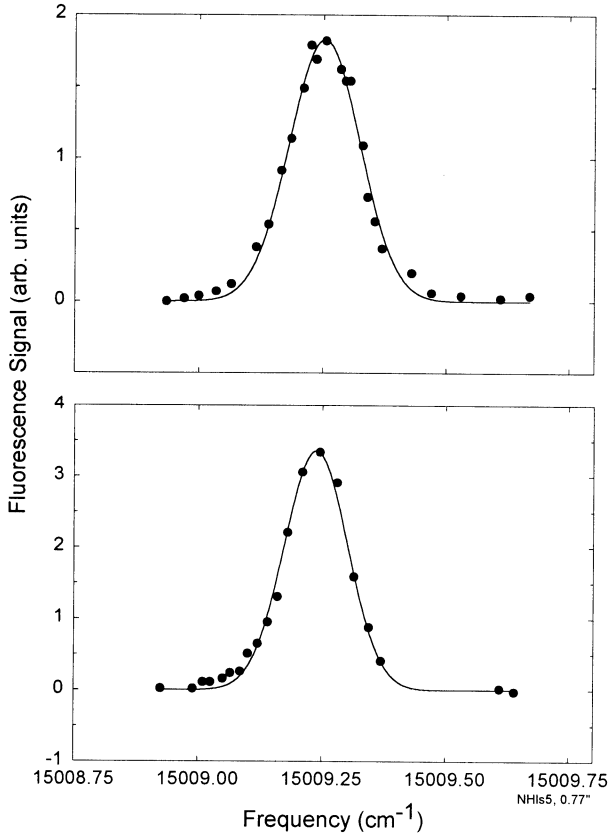

Figure 2. NH lineshapes for $R_2(7)$ 0-0 obtained on centerline at z=0.18 cm (top) and 1.96 cm (bottom).

lineshapes. The lineshape peaks are red-shifted about 0.22 cm^{-1} from the known transition frequency of $R_2(7)$ v'=0←v"=0, because of the NH Doppler shift at its axial plume velocity.

The temperatures indicated in Table 2 were obtained from the relation

$$\Delta\nu \cong \sqrt{\Delta\nu_D^2 + \Delta\nu_I^2 + \Delta_P^2} \ , \qquad (8)$$

and Equs. 6-8. Doppler broadening largely determines the lineshape when the laser pulse energy is low. For the conditions of the experiment, the contribution of power broadening to the linewidths was roughly estimated at 7%. In contrast to the H atom, the DC Stark effect for NH is relatively small[18] and was neglected in the analysis. Self-absorption was also neglected, since no evidence of it was observed.

The lineshapes for N atom obtained by the DSMC method are plotted in Fig. 3, and the corresponding temperatures are included in Table 2. A direct comparison between parallel and perpendicular temperatures for DSMC and experimental data could not be made, since all of the parallel lineshapes in the experimental data set were believed to be substantially power broadened.

The peak LIF signal at the center of the lineshape was measured as a function of axial coordinate, on-centerline, and is plotted in Fig. 4. Like the hydrogen atom case, the function is non-monotonic. The NH signal peaks at 1.4 cm downstream from the exit plane whereas H atom signal peaked at 0.8 cm. The unexpected existence of such a prominent peak at z = 1.4 cm may result from a high production rate of NH at this location. An NH formation rate on the order of 10^{19} $cm^{-3}s^{-1}$ is anticipated near the exit plane, which can create the required 10^{13} cm^{-3} population density within 1 μs.

The DSMC density profile is also shown in Figure 4 for comparison. The DSMC result gives density directly, so that for direct comparison the experimental result should be multiplied at each data point by the corresponding radial linewidth. The linewidth-corrected profile obtained from applying DSMC linewidth factors, is also shown in the Figure. Quenching is also estimated to account for about a factor of 2 correction, but nearly an order of magnitude discrepancy remains. As already mentioned, the most plausible explanation for this is the rapid formation of NH directly in the plume, such that the centerline density actually increases from the exit plane to z = 1.4 cm despite the geometric plume expansion.

The peak of the measured axial velocity distribution, in m/s, is plotted in Fig. 5. The plot also indicates the DSMC results obtained for N atom. A reduction in peak flow velocity occurs with increasing distance from the exit plane, on centerline, in each case. The experimental peak velocity is 0.5 - 1 km/s lower and suggests a larger velocity decrease with distance. The fall-off of the peak with radial coordinate is more abrupt than for axial coordinate, as expected, but the DSMC and experimental axial velocities are in qualitative rather than quantitative agreement.

NH is left with substantial internal and translational energy as a byproduct of at least the majority of mechanisms which form it in the arcjet plume. Mechanisms of formation which operate at substantial rates and which may leave residual energy in the NH product include dissociative electron impact, dissociative electron recombination, bimolecular reaction, and photolysis.[11,19,20] Normally, one would expect that ground state species are relatively equilibrated with the translational and rotational degrees of freedom in the background gas. This is probably the case for NH, with excited states in nonequilibrium with each other and the ground state.[21,22] In the extreme case, even the velocity distribution of an excited state can be in nonequilibrium.[23]

Because NH is relatively massive its velocity distribution will tend to be widened by collisions with the relatively fast, abundant species of H and H_2. This process leads to a DSMC rotational temperature for N_2 greater than

4000K with the H_2 rotational temperature about 2000K lower as shown in Fig. 6. The vibrational temperatures are

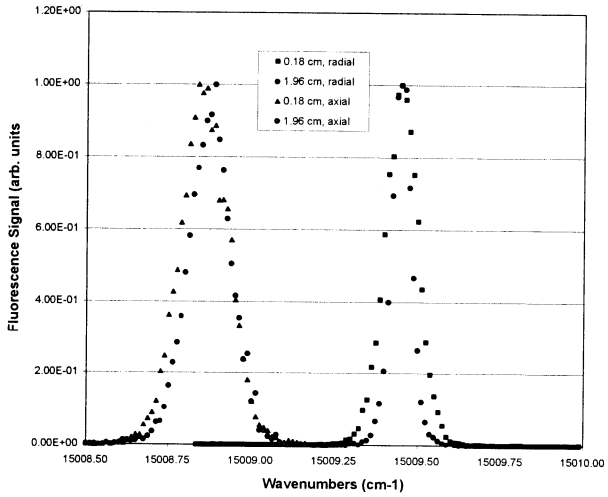

Figure 3. N atom parallel and perpendicular lineshapes from DSMC results.

predicted to follow similar trends, according to the DSMC results. The rotational temperature of NH was studied in v=0,1 of the ground electronic state. The relative intensities of $Q_2(J)$ and $R_2(J)$ series were measured, keeping laser intensity a constant. A slow drop in rotational temperature with z is believed to exist, as the trend is also indicated by the DSMC data. The plots of Fig. 7 were made according to Equ. 3, and approximately yield the temperatures given in Table 3.

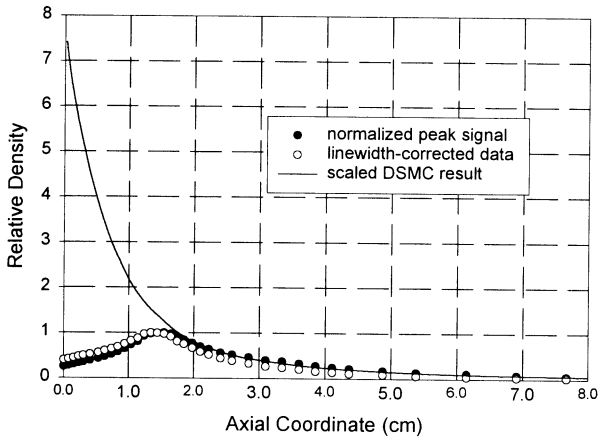

Figure 4. Axial NH and N atom profiles, from experimental and DSMC data.

The upper state lifetime depends on vibrational state as well as rotational state, although the best experimental and theoretical results differ.[7,8] Using the radiative and predissociative rates of the theoretical computations, which are probably the best available, resulted in small rotational temperature corrections on the order of 100K which are reflected in the values of Table 3. The corrections were smaller than the experimental uncertainty, and are themselves approximate due to the uncertainty in radiative and predissociative rates, and the spatially-dependent quenching rate.

No difference was found between v=0 and v=1 rotational temperatures, to within experimental error.

Vibrational "temperature" was also determined, from the ratio of 2-2 and 1-1 transitions to 0-0. These transitions are known to have similar oscillator strengths, except that the 2-2 case suffers from predissociation in the upper state which reduces the state lifetime. Corrections were made reflecting the predissociation effect. The vibrational and rotational temperatures were found to be remarkably similar.

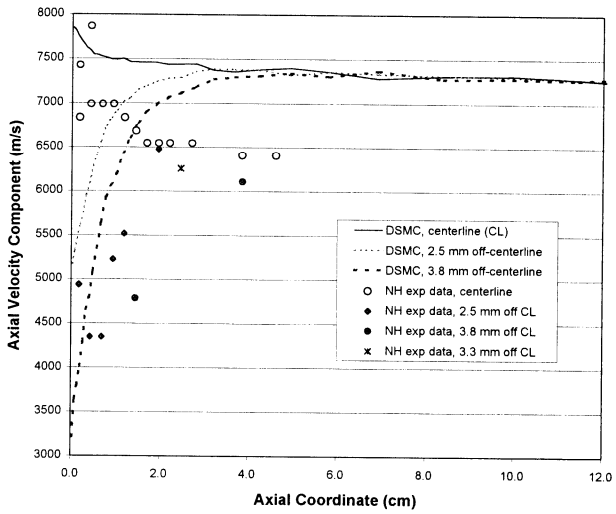

Figure 5. Comparison of experimental (symbols) and DSMC data (lines) for peak axial velocity component.

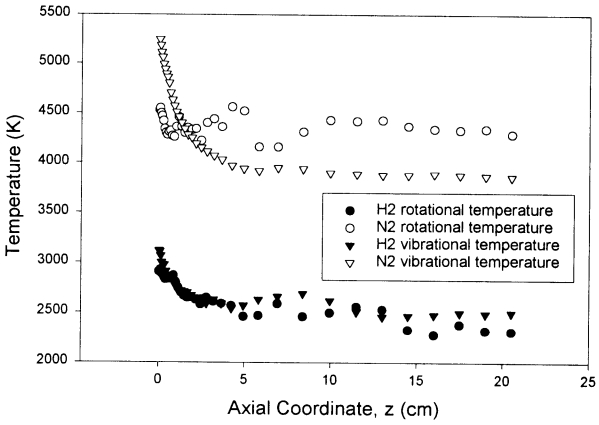

Figure 6. DSMC results for rotational and vibrational temperatures of H_2 and N_2.

Radial profiles of peak signal intensity are plotted in Fig. 8. These were converted to density profiles using the DSMC velocity distribution functions for N atom, along the radial cuts. The result in shown in Fig. 9. Excellent agreement was obtained at z = 1.96 and 3.23 cm, but it is apparent that the experimental profile at z = 0.30 cm is slightly wider than the DSMC profile. This can be explained as a quenching effect, which flattens the peak with respect to the shoulders.

From the dissociation fraction of H_2 or the absolute density of H atoms determined elsewhere,[17,24,25] one of the major power loss mechanisms of the arcjet can be estimated. The dissociation fraction determined by mass spectrometry was 14.3%.[17] At the 6.0 mg/s flow rate of H_2, the flow rate of dissociated molecules is 2.6×10^{20} s^{-1}, corresponding, at

4.48 eV/molecule, to a power loss of 184W. For N_2 the dissociation fraction is 10.9%, corresponding to a flow rate of dissociated molecules equal to 9.5×10^{19} s^{-1} and,

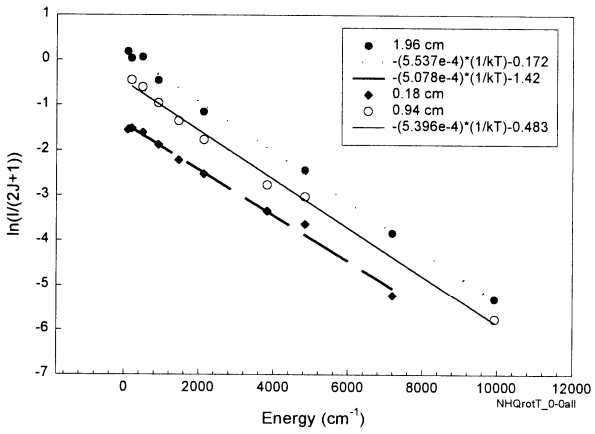

Figure 7. Rotational temperature determinations using the experimental data and Equ. 3.

at 7.37 eV/molecule, a power loss of 112W. Dissociation therefore accounts for just 18% (296W/1660W) of the total arcjet power input. This is a much smaller percentage than the 64% that has been proposed recently for the hydrogen arcjet.[25]

Other power losses are thermal conduction and radiation (across the entire spectrum), molecular rotation and vibration, electronic excitation and ionization. On the basis of the available MR509A data, each of these can now be estimated (see Table 3), since we have useful knowledge concerning the rotational, translational, and vibrational temperatures of all major species, ionization and excitation fractions, mole fractions, etc. The sum of all non-translational power sinks is about 590W. The kinetic power flux determined by mass spectrometry was 1007 ± 171 W.[17] The direct measurement of arcjet thrust on the standard MR509 arcjet came up with 580W thrust power.[3,17] Taking the average and subtracting from 1007, 427 ± 171 W of waste kinetic power is obtained, assuming the error bars are small for the direct thrust measurement. This sink arises from plume divergence and axial velocity distributions. In addition, velocity distributions (and their associated kinetic energy) transverse to the arcjet-detector axis are not observed by the mass spectrometer. The experimental uncertainty associated with the total waste kinetic power is high, but non-useful kinetic power is obviously one of the largest single categories for MR509A power loss. Adding all of the sinks together we have a sum of about 1660W, which is in fortuitously close agreement with the arcjet input power. This is the first time that power losses have been determined to this level of accuracy, or that the sum has been in agreement with the known power input.

The discrepancy in H atom density values obtained for the hydrogen arcjet from DSMC and the experimental approach of Ref. 25, may now be resolved. The DSMC result is the more accurate one. The experimental H_2 dissociation fraction was high, and most of the waste kinetic power was neglected in the Wysong and Pobst[25] analysis.

Near-field plume data is valuable for the understanding of the arcjet flow and performance properties. The study of spacecraft plume impingement and torquing, as well as contamination and thermal loading, are best accomplished via DSMC calculations. Validation and improvements in code accuracy are accomplished by incorporating the results of plume measurements into the modeling analysis.[26]

Acknowledgments

Thruster operations support was provided by D. Zube, J. English, and S. Crook of PRIMEX Aerospace, and J. Pollard, M. Worshum, L. Ortega, and E. Fournier of Aerospace Corporation. E. Beiting, J. Pollard, and R. Cohen provided valuable assistance in other aspects of the project. This manuscript is a revision of a 1998 report to MELCO, and its preparation was partially funded by the Aerospace IR&D program.

References

1. Zube, D.M., Fye, D., Masuda, I., and Gotoh, Y., "Low Bus Voltage Hydrazine Arcjet System for Geostationary Satellites," AIAA Paper 98-3631, 34th Joint Propulsion Conf., Cleveland, July 1998.

2. Martinez-Sanchez, M., and Pollard, J.E., "Spacecraft Electric Propulsion," *J. Propulsion and Power*, Vol. 14, No. 5, 1998, pp. 688-699.

3. Smith, R.D., Roberts, C.R., Aadland, R.S., Lichtin, D.A., and Davies, K., "Flight Qualification of the 1.8 kW MR-509 Hydrazine Arcjet System," IEPC Paper 97-081, Aug. 1997.

4. Altkorn, R. and Zare, R.N., "Effects of Saturation on Laser-Induced Fluorescence Measurements of Population and Polarization," *Ann. Review of Physical Chemistry,* Vol. 35, 265 (1984).

5. Smith, W.H. and Liszt, H.S., "Franck-Condon Factors and Absolute Oscillator Strengths for NH, SiH, S_2, and SO," *J. Quantitative Spectroscopy and Radiative Transfer*, Vol. 11, No. 45, 1971.

6. Citron, M.L., Gray, H.R., Gabel, C.W., and Stroud, C.R., Jr., "Experimental Study of Power Broadening in a Two-Level Atom," *Physical Review A*, Vol. 16, No. 4, 1977, pp. 1507-12.

7. Smith, W.H., Brzozowski, J., and Erman, P., "Lifetime Studies of the NH Molecule: New Predissociations, the Dissociation Energy, and Interstellar Recombination," *J. Chemical Physics*, Vol. 64, No. 11, 1976, pp. 4628-33.

8. Patel-Misra, D., Parlant, G., Sauder, D.G., Yarkony, D.R., and Dagdigian, P.J., "Radiative and Nonradiative Decay of the NH(ND) A $^3\Pi$ Electronic State: Predissociation Induced by the $^5\Sigma^-$ State," *J. Chemical Physics*, Vol. 94, No. 3, 1991, pp. 1913-1922.

9. Crofton, M.W., Moore, T.A., Boyd, I.D., Masuda, I., and Gotoh, Y., "Near-Field Measurement and Modeling Results for a Flight-Type Arcjet: H Atom," IEPC Paper 99-048, 26th International Electric Propulsion Conf., Kitakyushu, Oct 1999.

10. Garland, N.L., Jeffries, J.B., Crosley, D.R., Smith, G.P., and Copeland, R.A., "NH A $^3\Pi_i$ Quenching at 1400K," *J. Chemical Physics*, Vol. 84, No. 9, 1986, pp. 4970-4975.

11. Dodd, J.A., Lipson, S.J., Flanagan, D.J., Blumberg, W.A.M., Person, J.C., and Green, B.D., "NH (X $^3\Sigma^-$, v=1-3) Formation and Vibrational Relaxation in Electron-Irradiated Ar/N_2/H_2 Mixtures," *J. Chemical Physics*, Vol. 94, No. 6, 1991, pp. 4301-4310.

12. Butler, G.W., Boyd, I.D., and Cappelli, M.A., "Nonequilibrium Flow Phenomena in Low Power Hydrogen Arcjets," Paper 95-2819, AIAA Joint Propulsion Conference, San Diego, CA, July 1995.

13. Bird, G.A., *Molecular Gas Dynamics and the Direct Simulation of Gas Flows*, Oxford University Press, 1994.

14. Boyd, I.D., "Monte Carlo Simulation of Nonequilibrium Flow in Low Power Hydrogen Arcjets," *Physics of Fluids*, Vol. 9, 1997, pp. 3086-3095.

15. Boyd, I.D., "Extensive Validation of a Monte Carlo Model for Hydrogen Arcjet Flow Fields," *J. Propulsion and Power*, Vol. 13, 1997, pp. 775-782.

16. Brazier, C.R., Ram, R.S., and Bernath, P.F., "Fourier Transform Spectroscopy of the A $^3\Pi$ - X $^3\Sigma^-$ Transition of NH," *J. Molecular Spectroscopy,* Vol. 120, 1986, pp. 381-402.

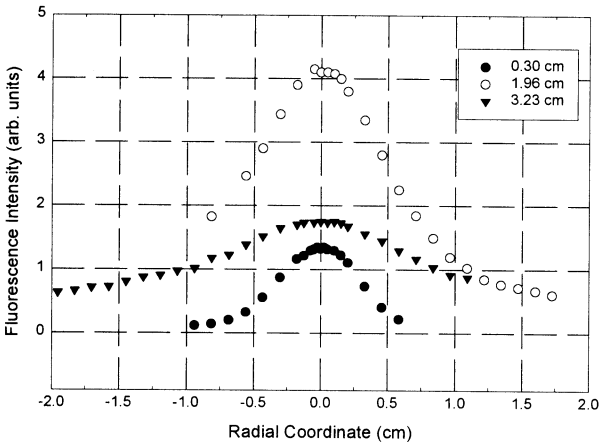

Figure 8. Radial profiles of peak intensity.

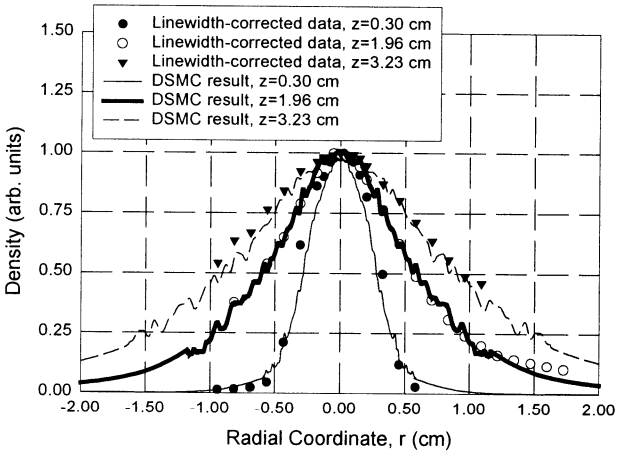

Figure 9. DSMC radial density profiles for nitrogen atom (lines), compared to linewidth-corrected NH experimental data (symbols).

17. Pollard, J.E., Masuda, I., and Gotoh, Y., "Plume Mass Spectrometry and Calorimetry with a Hydrazine Arcjet Thruster," IEPC Paper 99-041, 26th International Electric Propulsion Conf., Kitakyushu, Oct 1999.
18. Irwin, T.A.R., and Dalby, F.W., "Experimental Determination of the Dipole Moments of the Degenerate States of NH," *Canadian J. Physics*, Vol. 43, 1965, pp. 1766-75.
19. Tokue, I., Fujimaki, A., and Ito, Y., "Formation and Internal Energy Distributions of the NH (A,c) Radicals by Electron-Impact Dissociation of Hydrazine and Methylamine," *J. Physical Chemistry*, Vol. 88, 1984, pp. 6250-54.
20. Haak, H.K. and Stuhl, F., "ArF (193 nm) Laser Photolysis of HN_3, CH_3NH2, and N2H4: Formation of Excited NH Radicals," *J. Physical Chemistry*, Vol. 88, No. 16, 1984, pp. 3627-33.
21. Crofton, M.W., Welle, R.P., Janson, S.W., and Cohen, R.B., "Temperature, Velocity and Density Studies in the 1 kW Ammonia Arcjet Plume by LIF," AIAA Paper 92-3241, July 1992.
22. Zube, D.M., and Myers, R.M., "Thermal Nonequilibrium in a Low-Power Arcjet Nozzle," *J. Propulsion and Power*, Vol. 9, No. 4, 1993, pp. 545-552.
23. Kurawake, J., and Ogawa, T., "Translational Energy Distributions and Production Mechanisms of the Excited Hydrogen Atom (n=3,4) Produced in e-NH_3 Collisions," *Chemical Physics*, Vol. 86, 1984, pp. 295-301.
24. Pollard, "Arcjet Diagnostics by XUV Absorption Spectroscopy," AIAA Paper 92-2966, 23rd Plasmadynamics and Lasers Conf., Nashville, July 1992.
25. Wysong, I.J., and Pobst, J.A., "Quantitative Two-Photon Laser-Induced Fluorescence of Hydrogen Atoms in a 1 kW Arcjet Thruster," *Applied Physics B*, Vol. 67, 1998, pp.193-205.
26. Nelson, D.A., Gotoh, Y., and Masuda, I., "A Simplified Model for the Prediction of Arcjet Plumes," IEPC Paper 99-043, 26th International Electric Propulsion Conf., Kitakyushu, Oct 1999.

Table 3. NH rotational and vibrational temperatures

(r,Z) cm	Rotational (K), v"=0 Q_2 (J) series	Rotational (K), v"=1 R_2(J) series	Vibrational (K) (1-1)/(0-0)	Vibrational (K) (2-2)/(0-0)
0,0.18	2980 ± 290	2800 ± 500	2750 ± 200	3090 ± 400
0,0.94	2750 ± 250	-	-	-
0,1.96	2690 ± 160	-	2720 ± 200	2 780 ± 300
0,4.11	-	-	2570 ± 300	-

Table 4. Estimated power sinks (Watts) for the MR509A at the 1660W, 46.4 mg/s operating point.

Molecular Dissociation	Transverse Thermal Kinetic†	Molecular Rotation and Vibration	Thermal Conduct-ion and Radiation	Waste Kinetic Power‡	Ionization and Excitation	Thrust Power
184 + 112 = 296	60	60 + 60 = 120	160	430 ± 170	10	580

†Kinetic energy not measured by mass spectrometry.
‡Difference between measured kinetic power from mass spectrometry, and thrust power from direct thrust measurement.